As(III) adsorption on Fe-Mn binary oxides: are manganese and iron oxides synergistic or 1 antagonistic for arsenic removal?

by Zhen, Q., Hou, J., Hartley, W., Ren, L., Wang, M., Tu, S. and Tan, W.

DOI: https://doi.org/10.1016/j.cej.2020.124470

Zhen, Q., Hou, J., Hartley, W., Ren, L., Wang, M., Tu, S. and Tan, W. 2020. As(III) adsorption on Fe-Mn binary oxides: are manganese and iron oxides synergistic or 1 antagonistic for arsenic removal? *Chemical Engineering Journal.*
16 February 2020

As(III) adsorption on Fe-Mn binary oxides: are manganese and iron oxides synergistic or antagonistic for arsenic removal?

Qian Zheng,[1] Jingtao Hou,[1,*] William Hartley,[2] Lu Ren[3], Mingxia Wang,[1] Shuxin Tu,[1,*] Wenfeng Tan[1]

[1] College of Resources and Environment, Huazhong Agricultural University, Wuhan 430070, China.

[2] Crop and Environment Sciences Department, Harper Adams University, Newport, Shropshire, TF10 8NB, United Kingdom.

[3]School of Civil Engineering, Suzhou University of Science and Technology, Suzhou 215009, China

ABSTRACT. Fe-Mn binary oxides are ubiquitous in the natural environment and have attracted increasing interest due to their high removal capacity for As(III), as well as their important role in the natural cycling of arsenic. Although numerous studies have characterized the respective roles of Fe and Mn oxides in As(III) removal, the relationship between different Fe-Mn binary oxides for As(III) removal has not been fully explored. In this study, three Fe-Mn binary oxides containing either ferrihydrite, hematite or goethite, were used to evaluate their adsorption capacities for As(III) in comparison with their corresponding single Fe and Mn oxide forms. We utilized spectroscopic techniques of *in situ* flow ATR-FTIR and XPS combined with a Donnan reactor, where Fe and Mn oxides were isolated by a semi-permeable membrane through which arsenic could pass, to investigate the dynamics and speciation transformation of As(III) within mixed Fe and Mn oxides systems. The result showed that the synergistic effect, as well as antagonistic effects, between Fe and Mn oxides, was present in Fe-Mn binary oxides for As(III) removal. An obvious increase in As(III) removal with hematite, containing Fe-Mn binary oxides, and a decrease in ferrihydrite, containing Fe-Mn binary oxides, was attributed to As(III) oxidation mediated by Mn oxides as well as the difference in arsenic adsorption affinity in Fe oxides, evidenced by ATR-FTI R and XPS analyses. The findings of this work provide a new understanding of the fate of arsenic within mixed systems, which is very important for targeted application of Fe-Mn binary oxides

in treating real arsenic contaminated groundwater.

INTRODUCTION

Arsenic (As) is a common metal(loid) element that has gained much concern due to its high toxicity and carcinogenicity [1, 2]. In order to reduce the associated health risks, a guideline limit of 10 μg L^{-1} As in drinking water was set by the World Health Organization (WHO) [3]. In the natural environment, As is mainly present as inorganic forms, existing in two predominant species, arsenite [As(III)] and arsenate [As(V)] [1]. Arsenite is the major As species in reduced environments, possessing greater toxicity, but having a weaker affinity to metal oxides compared to As(V). Arsenate mainly exists in well-oxygenated environments [1, 4]. The strategy for oxidation of As(III) coupled with sorption of the formed As(V), using metal binary oxides as adsorbents, has been intensively investigated for treating As contaminated groundwater [2].

The reported binary oxides include Ce-Mn [5-7], Zr-Mn [8, 9], Ti-Mn [10-12], Fe-Mn [13-16] and Al-Mn [17, 18] etc. Among the series of binary oxides, Fe-Mn binary oxide, which is inexpensive and environmentally benign, has attracted much interest as a promising adsorbent for As removal, especially for As(III). Arsenite removal on Fe-Mn binary oxides reportedly follows an oxidation/adsorption mechanism, in which As(III) is oxidized to As(V) by manganese oxides, and the formed As(V) subsequently being adsorbed by the iron oxides [19-22]. Therefore, the existence of synergistic effects between manganese oxides (oxidants) and iron oxides (adsorbents) in Fe-Mn binary oxides, for As(III) removal, is widely accepted. However, several studies have reported that some iron (hydr-)oxides demonstrated lower adsorption capacities toward As(V) than As(III) [23-25]. For example, Zhang et al evaluated As(III) and As(V) adsorption capacities on amorphous ferrihydrite, and revealed that adsorption performance of As(III) on amorphous ferrihydrite was 2.15 times greater than that of As(V)

[24]. Wen et al also observed that iron hydroxide colloids showed As(III) adsorption capacity to be higher than that of As(V) [25]. Therefore, oxidation of As(III) by manganese oxides may be detrimental for As(III) removal. In principle, the type and content of iron (e.g., ferrihydrite, goethite, and hematite) and manganese oxides in both naturally occurring and synthesized Fe-Mn binary oxides are rather different, which depend on the natural environment as well as their preparation conditions. Although the respective roles of Fe and Mn oxides in As(III) removal have been characterized in previous studies [19, 22, 24, 26-28], the working relationship between Fe and Mn oxides with different Fe-Mn binary oxides is not fully understood. It is still unclear whether antagonistic and/or synergistic effects occur in Fe-Mn binary oxides during As removal. Elucidating these effects is very important for targeted application of Fe-Mn binary oxides in treating real As contaminated groundwater.

In this study, three Fe-Mn binary oxides containing either ferrihydrite, goethite or hematite, were synthesized using a superficial co-precipitation reaction. Arsenite adsorption capacities of the different Fe-Mn binary oxides were tested for comparison with their corresponding single Fe and Mn oxides. To illustrate the possible working relationships between Fe and Mn in the different binary oxides, we examined As(III) dynamics using a Donnan reactor composed of two reaction cells separated by a semi-permeable membrane, where Fe and Mn oxides were placed in two chambers, respectively.

MATERIALS AND METHODS

Materials. As_2O_3 and $Na_3AsO_4 \cdot 12H_2O$ were used to prepare As(III) and As(V) stock solutions, respectively. The As(III) and As(V) working solutions were prepared by diluting the corresponding stock solutions using deionized water. Manganese oxide samples used in this study were purchased from Sinopharm group chemical reagent co., LTD, China. All reagents were of analytical grade. A

polycarbonate semi-permeable membrane with a diameter of 100 mm was used in the Donnan reactor (Kenker Co., USA).

Sample Preparation. Ferrihydrite-containing Fe-Mn binary oxides were synthesized according to Zhang et al [29], using co-precipitation but with the addition of $MnCl_2$. Typically, $Fe(NO_3)_3 \cdot 9H_2O$ (0.1 M) (500 mL) and $MnCl_2$ (0.5 M) (60 mL) were thoroughly mixed together with NaOH (1M) (330 mL) using a magnetic stirrer until the solution pH reached 7 ~ 8. After stirring for 2 h, the precipitates were washed several times with deionized water until conductivity was lower than 20 mS cm^{-1}. The samples were then freeze-dried and subsequently stored at 4 ºC until required.

Goethite-containing Fe-Mn binary oxides were prepared using a similar method [30]. Typically, $Fe(NO_3)_3 \cdot 9H_2O$ (1 M) (100 mL) and $MnCl_2$ (0.5 M) (60ml) were thoroughly mixed. NaOH (5 M) (180 mL) was then added and constantly stirred using a magnetic stirring. The suspension was diluted to a volume of 2 L with distilled water, sealed with plastic wrap, and then placed in an oven at 70 ºC for 60 h. The precipitate was washed with deionized water, dried at 60 ºC for 1 day, and subsequently stored at 4 ºC until required.

Hematite-containing Fe-Mn binary oxides were prepared according to the method of Connell and Schwertamnn, except for the addition of $MnCl_2$ [31]. Typically, $Fe(NO_3)_3 \cdot 9H_2O$ (40 g) was added to 500 mL of 90 ºC deionized water in a 1000 mL beaker with constant magnetic stirring. $MnCl_2$ (0.5 M), (60mL), KOH (1 M) (300 mL) and $NaHCO_3$ (1 M) (50 mL) were preheated to 90 ºC and subsequently added to the above suspension. The beaker was sealed with plastic wrap and transferred to a 90 ºC oven . After 48 h, the precipitate was washed with deionized water several times, dried at 60 ºC, and stored at 4 ºC until required.

Preparation of the single ferrihydrite, goethite and hematite samples were the same as their

90 corresponding binary oxides but with the exception of no $MnCl_2$ addition.

91 **Sample Characterization.** X-ray diffraction (XRD) patterns for the different iron oxides and manganese
92 oxides were tested on a Bruker D8 ADVANCE X-ray diffractometer using Ni-filtered Cu Ka radiation.
93 Scanning electronic microscopy (SEM) images and energy dispersion spectrum (EDS) data were
94 obtained using a QUANTA FEG 450 electron microscope. Nitrogen adsorption–desorption isotherms
95 were obtained using a Micromeritics ASAP 2000 surface area analyzer. The spectra generated by X-ray
96 photoelectron spectrometry (XPS) spectra of the samples before and after reaction with As(III) in Donnan
97 experiments were collected using a VG Multilab 2000 X-ray photoelectron spectrometer with Mg Ka
98 radiation. Some selected samples were freeze-dried before being characterized by XPS.

99 **As(III) Oxidation Experiment.** As(III) oxidation on manganese oxide was performed on a thermostatic
100 shaker with a velocity of 200 rpm at 25 °C. The initial As(III) solution was 1.33 μM with an ionic strength
101 of 0.1 M $NaNO_3$ and a pH of 7.0 ± 0.1 adjusted by adding appropriate HCl or HNO_3. To start, 0.01 g of
102 manganese oxide were rapidly added into 1.33 μM of As(III) working solution in a 150 mL Erlenmeyer
103 flask. At set specific time intervals, the suspensions were filtered through a 0.22 μm membrane filter.
104 The concentration of total As and As(III) species were tested on an atomic fluorescence spectrometer
105 (AFS-9700) according to the detection method reported by Hong et al [32]. The As(V) concentration in
106 solution was obtained by subtracting the As(III) concentration from the total As concentration.

107 **Arsenic Adsorption Experiment.** The arsenic adsorption performance of Fe (hydr-)oxide, Mn oxide,
108 the Fe-Mn binary oxides, and mixed Fe and Mn oxides, were investigated using adsorption isotherms at
109 pH 7.0 in a dark environment. All adsorption experiments were performed on a thermostatic shaker with
110 a velocity of 200 rpm at 25 °C for 24 h. The ion strength in all bath experiments was adjusted to 0.1 M
111 using $NaNO_3$. Typically, 0.01g of Fe oxide, Mn oxide, or Fe-Mn binary oxide were added into 100 mL

112 of arsenic solution with a series of concentrations ranging from 0.13 to 133.3 μM in a 150 mL Erlenmeyer
113 flask. During the adsorption experiment, solution pH was adjusted every 6 h using HCl and NaOH to
114 7.0 ± 0.1. After 24 h, the suspensions were withdrawn and filtered through a 0.22 μm membrane filter.
115 Arsenic adsorption performance of the mixed Fe and Mn oxides was also tested using the same treatment
116 as that of single Fe oxide except for the addition of 0.01 g of Mn oxide. The amount of adsorbed As on
117 iron oxide surfaces was obtained by subtracting the residual As concentration from the initial As
118 concentration divided by the weight of Fe oxide adsorbent. All batch adsorption experiments were carried
119 out in triplicate.

120 **Donnan Experiment.** The Donnan reactor used in this study was composed of two reaction cells
121 separated by a semi-permeable membrane (Figure 1) [30]. The reaction cells were constructed using
122 acrylic pipes. A 0.1μm polycarbonate filter was used as the semi-permeable membrane. Before the
123 experiment, the Donnan reactor was carefully tested for leakages by adding water into the two reaction
124 cells. To start, 0.2 g of Fe oxide and 0.2 g of Mn oxide were placed into two reaction cells, respectively
125 (Figure 1). To determine the relationship between Fe and Mn oxides for As(III) removal, two experiments
126 were designed. For the first experiment, only As(III) was added into the Fe oxide chamber (Figure S1A,
127 **see supporting information**), and the second only As(III) was added into the Mn oxide chamber (Figure
128 S1B). Considering that the two iron oxides have different adsorption capacities for As removal,
129 evidenced from the adsorption experiment, the initial As(III) concentration in ferrihydrite-Mn oxide and
130 hematite-Mn oxide systems was set as 133.3 and 26.7 μM, respectively. The initial pH in all reactions
131 was set to 7.0 ± 0.1. Following the reaction, pH was monitored and adjusted using HCl and NaOH. The
132 ionic strength in the two cells was adjusted to 0.1 M using $NaNO_3$. The aqueous As concentration (c) at
133 a given time in the Donnan reactor was calculated according to the following formula.

$$c = \frac{c_1 + c_2}{2} \qquad (1)$$

Where c_1 and c_2 represent the As concentration in Fe and Mn oxide chambers, respectively (μmol L^{-1}).

***In situ* Flow Attenuated Total-reflectance Fourier Transform Infrared Spectroscopy (ATR-FTIR) Experiments.** *In-situ* flow ATR-FTIR was used to measure the adsorption/oxidation of As(III) on single Fe oxides and mixed Fe and Mn oxides, thereby explaining the respective roles of Fe and Mn oxides in different Fe-Mn binary oxides for As(III) removal. Typically, 0.05 g of iron oxide was added to 1 mL of deionized water for ultrasonic dispersion for ~ 5 min. The obtained suspension was covered on ZnSe crystals and dried at room temperature for 12 h. Before the experiment began, 0.1 M of $NaNO_3$ solution with pH of 7.0 was used as a background electrolyte, to pump through the iron oxide covered ZnSe crystals at a flow rate of 1.0 mL min^{-1} , thereby balancing the functional groups on iron oxides. After 90 min, 1 mM of As(III) solution (pH =7.0) was continuously pumped through the iron oxide covered ZnSe crystals at a flow rate of 0.5 mL min^{-1}. *In-situ* flow ATR-FTIR experiments of the mixed iron and manganese oxides reacted with As(III) were performed using the same treatment as that of the iron oxide except for the addition of 0.05 g Mn oxide. As(III) adsorption/oxidation was monitored by a DTGS detector with an infrared spectrum acquisition. The scanning range, IR resolution, and scanning times were set to 4000 ~ 600 cm^{-1}, 4 cm^{-1}, and 512, respectively. The OPUS software was employed for data processing.

RESULTS AND DISCUSSION

Characterization of Fe (hydr-)oxides, Mn oxide and Fe-Mn binary oxides. The X-ray diffraction (XRD) patterns of the Fe (hydr-)oxides, Mn oxide and Fe-Mn binary oxides are revealed in Figure S2. XRD analysis revealed that Fe oxides used in this study were indexed to the pure structure of 2-line ferrihydrite [14], hematite [JCPDS 13-0534], and goethite [JCPDS 02-0282], respectively (Figure S2A). Mn oxide was typical of the manganite phase [JCPDS 42-1316]. Fe oxide phases in different Fe-Mn binary oxides were ferrihydrite, hematite, and goethite, respectively (Figure S2B). No Mn oxide phase was observed in all Fe-Mn binary oxides due to the low initial $MnCl_2/Fe(NO_3)_3$ reactant molar ratio in all reaction systems. The EDS data revealed that both Fe and Mn elements coexisted (Table S1, **see supporting information**), suggesting Mn oxide was successfully incorporated into all Fe-Mn binary oxides. SEM images revealed that the surface of ferrihydrite-containing Fe-Mn binary oxides (denoted as Fh-MnO_x) was very rough, containing bumps and hollows, relative to that of hematite-containing Fe-Mn binary oxides (denoted as Hem-MnO_x) (Figure S3A and C), suggesting that the former may supply more active sites than the latter for As adsorption. Goethite-containing Fe-Mn binary oxides (denoted as Goe-MnO_x) showed typical needle-like morphology, indicating that goethite had successfully been incorporated into Goe-MnO_x samples (Figure S3B). The BET surface areas of the samples, determined by fitting their N_2 adsorption/desorption curves, are displayed in Table S1. Ferrihydrite showed a specific surface area (247.0 m^2 g^{-1}) far greater than goethite (143.3 m^2 g^{-1}) and hematite (38.9 m^2 g^{-1}). The high surface area of ferrihydrite was attributed to its low crystallinity compared to both goethite and hematite, which had been observed in previous work. The specific surface areas of Fh-MnO_x, Goe-MnO_x, and Hem-MnO_x samples were 266.4, 213.3, and 32.8 m^2 g^{-1}, respectively.

178

179 **Arsenic adsorption in single Fe oxide and mixed Fe and Mn oxides.** Figure 2 exhibits the adsorption
180 isotherm profiles of Fe oxides, Mn oxide, and mixed Fe and Mn oxides for As removal. The Langmuir
181 and Freundlich models were used to describe the adsorption isotherms and the corresponding fitting
182 results are displayed in Table S3. We used a maximum adsorption amount calculated from the Langmuir
183 model for comparing adsorption capacities. As shown in Figure 2 and Table S3, three iron oxides
184 ferrihydrite, goethite, and hematite, which exist extensively in terrestrial environments, showed obvious
185 differences in their adsorption capacities for both As(III) and As(V) [23, 24, 33]. Ferrihydrite possessed
186 the greatest adsorption capacity for both As(III) and As(V), followed by goethite and hematite.
187 Interestingly, the three iron oxides exhibited different affinities for As(III) and As(V) species. For single
188 hematite, its maximum As(III) adsorption capacity (51.2 μmol g^{-1}) was lower than that of As(V) (65.3
189 μmol g^{-1}) (Figure 2a). For goethite, its maximum As(III) adsorption capacity (112.8 μmol g^{-1}) was slightly
190 greater that of As(V) (102.7 μmol g^{-1}) (Figure 2b). However, for ferrihydrite, the maximum As(III)
191 adsorption capacity (871.5 μmol g^{-1}) was much greater than that of As(V) (493.8 mg g^{-1}) (Figure 2c).
192 Compared to iron oxides, manganese oxide possessed very low adsorption capacity for both As(III) and
193 As(V) removal (Figure S4), but extremely high oxidation activity for As(III) (Figure S5), suggesting that
194 manganese oxide mainly acts as an oxidant for oxidation of As(III) to As(V), rather than as an adsorbent
195 [34-37]. Therefore, based on the above results, we speculated that the working relationships between Fe
196 and Mn oxides in Fe-Mn binary oxides for As(III) removal, exist either synergistically, or antagonistically
197 in some cases. However, this observation was not clear in previous work, and still needs further
198 clarification.

199 In order to confirm our assumption, As(III) adsorption capacities of the mixed Fe and Mn oxides was

200 investigated for comparison with corresponding single Fe and Mn oxides (Figure 2). For mixed hematite
201 and Mn oxides, As(III) adsorption capacity was 90.9 μmol g^{-1} (Figure 3d), which was clearly greater than
202 those of single hematite (51.2 μmol g^{-1}) and Mn oxides (9.5 μmol g^{-1}), suggesting that the synergistic
203 effect between hematite and Mn oxide was present in promoting As removal in this case. For the mixed
204 goethite and Mn oxide, its As(III) adsorption capacity increased slightly to 116.3 μmol g^{-1} relative to
205 single goethite and Mn oxide, indicating that the additive effect between goethite and Mn oxide was
206 observed with a slight enhancement in As(III) removal. Remarkably, for mixed ferrihydrite and Mn oxide,
207 an obvious decrease in As(III) adsorption capacity (694.4 μmol g^{-1}) was evident, relative to that of single
208 ferrihydrite (871.5 μmol g^{-1}), suggesting antagonistic effects between ferrihydrite and Mn oxide at
209 decreasing As(III) removal. This result demonstrated that the synergistic effect, as well as antagonistic
210 effects, between Fe and Mn oxides, was present in Fe-Mn binary oxides for As(III) removal, which was
211 in agreement with our assumption.

212 The question is therefore, why do antagonistic effects between Fe and Mn oxides occurr in mixed
213 ferrihydrite and Mn oxide systems? There are two factors that affect As(III) removal. Firstly the change
214 in As species mediated by Fe or Mn oxides, thus altering the adsorption affinity of As to iron oxides.
215 Secondly, the Mn oxide adsorbed onto ferrihydrite surfaces, which occupies active sites for As(III)
216 adsorption. We examined the As(V) adsorption capacity of the mixed ferrihydrite and Mn oxide for
217 comparison with its corresponding single ferrihydrite (Table S2). The As(V) adsorption capacity of the
218 mixed ferrihydrite and Mn oxide was 452.0 mg g^{-1}, which was slightly lower than that of single
219 ferrihydrite (493.8 mg g^{-1}). This result suggested that Mn oxide adsorbed onto iron oxide surfaces has a
220 'littering effect' on the active sites which could be used for As(III) adsorption, and the transformation of
221 As species within the mixed Fe-Mn oxides system may play a vital role in As(III) removal.

222 We also evaluated the As(III) adsorption capacities of three Fe-Mn binary oxides containing
223 ferrihydrite (Fh-MnO_x), goethite (Goe-MnO_x), and hematite (Hem-MnO_x), respectively (Figure S6). The
224 three Fe-Mn binary oxides showed specific surface areas different from their corresponding single Fe
225 and Mn oxides. Specific As(III) adsorption capacities (per unit surface area of absorbent), representing
226 the intrinsic adsorption ability of Fe-Mn binary oxides, were therefore compared. As shown in Figure
227 S6a, the specific As(III) adsorption capacity of binary Hem-MnO_x samples (3.12 μmol m^{-2}) was greater
228 than that of single hematite (1.32 μmol m^{-2}). For binary Goe-MnO_x samples, the specific As(III)
229 adsorption capacity (0.62 μmol m^{-2}) was slightly lower than that of single goethite (0.78 μmol m^{-2})
230 (Figure S6b). For binary Fe-MnO_x samples, specific As(III) adsorption capacity (3.31 μmol m^{-2}) was
231 lower than that of single ferrihydrite (3.53 μmol m^{-2}) (Figure S6b). This further demonstrates that both
232 synergistic and antagonistic effects between Fe and Mn oxides in binary oxides exist for As(III) removal.
233 It is therefore very important to select suitable Fe-Mn binary oxides for treatment of real arsenic
234 contaminated groundwater.

235 ***In situ* flow ATR-FTIR.** To reveal the sorption and redox behaviors of As(III) within single iron oxide
236 and mixed Fe-Mn oxide systems, an *in situ* flow ATR-FTIR experiment was investigated (Figure 3).
237 Figure S7 reveals the FTIR spectra of pure As(III) and As(V) standards, where the IR absorption peak at
238 ~ 798 cm^{-1} corresponds to As(III) species, and those at ~ 817 and ~ 865 cm^{-1} are attributed to As(V)
239 species [38-40]. For single ferrihydrite reacted with As(III), the IR adsorption peak was approximately
240 789 cm^{-1}, which was assigned to As(III) species, and appeared to become stronger with increasing
241 reaction time (Figure 3a). However, the characteristic adsorption peak of As(V) was not obviously
242 observed in the entire reaction time, suggesting that As(III) had not transferred to As(V) by ferrihydrite
243 in this case. For single hematite reacted with As(III), As(III) was also the main As species adsorbed,

evidenced by the IR adsorption peak around 802 cm^{-1} (Figure 3b). However, the intensity of As(III) characteristic adsorption peak in hematite was not as strong as that in ferrihydrite, suggesting that the affinity of As(III) in ferrihydrite was stronger than that in hematite, which was in agreement with adsorption isotherm data. Interestingly, for mixed Fe and Mn oxide systems, two IR adsorption peaks at ~ 817 and ~798 cm^{-1}, which were assigned to As(III) and As(V) species, respectively, were observed simultaneously and became stronger with increasing reaction time (Figure 3c and d). This result revealed that Mn oxide led to the rapid transformation of As(III) to As(V), which may play an indirect role in controlling As adsorption on iron oxides.

Aqueous arsenic dynamics within Donnan reactor. To further illustrate the different working relationships between Fe and Mn oxides in Fe-Mn binary oxides for As(III) removal, we used a Donnan reactor, where the oxides were placed in two chambers separated by a semi-permeable membrane, to examine As adsorption kinetics by adding As(III) to one side of chamber (Figure S2). Ferrihydrite and hematite, which showed opposite adsorption affinities to both As(III) and As(V), were used to perform the Donnan experiment. Considering that As(III) oxidation by dissolved oxygen is very slow, the dissolved oxygen in this study was not further removed by introducing an inert gas [4, 41]. Arsenic concentration in the ferrihydrite chamber rapidly decreased after addition of As(III), whilst with Mn oxide there was a slight increase (Figure 4a), suggesting that most of the As(III) species may be rapidly adsorbed by ferrihydrite without further diffusion into the Mn oxide chamber. After 10 h, As concentration reached equilibrium in the two chambers (Figure 4a). However, As concentration in the Mn oxide chamber decreased slowly after addition of As(III) (Figure 4b). The decrease in As concentration in the Mn oxide chamber mainly depended on As diffusion transport between the neighboring chambers. Arsenite had undergone oxidation, diffusion, and adsorption, which was more

complex than when it was applied to the ferrihydrite chamber. Equilibrium was reached after ~ 36 h (Figure 4b). Addition of As(III) to the manganese oxide chamber reached an As concentration of 29.2 μmol L^{-1}, whereas in the ferrihydrite chamber only 20.0 μmol L^{-1} was reached (Figure S8a). This result indicates that the antagonistic effect between ferrihydrite and Mn oxide in Fe-Mn oxide systems may be attributed to pre-treatment of As(III) by Mn oxide.

In the hematite chamber, the decrease in As concentration was not as rapid as that in the ferrihydrite chamber (Figure 4c). This may be due to the weak adsorption of As(III) on hematite and the slow diffusion of As(III) into the Mn oxide chamber. Arsenite, in the Mn oxide chamber, had undergone oxidation, diffusion, and adsorption processes, and equilibrium was reached after ~ 24 h. Pretreatment of As(III) by Mn oxide also increased As removal in the hematite-Mn oxide system (Figure S8b). However, the aqueous As concentration in the Donnan reactor was close to each other with increasing reaction time. This observation could be explained by the high affinity of As(V) in hematite compared to As(III), which will be discussed further in XPS analysis (see **XPS analysis section**).

Surface analysis of Fe and Mn oxides in Donnan experiments. To reveal the evolution of surface speciation of Fe, Mn and As during the processes of As(III) sorption and redox in the Donnan reactor, the surface compositions of Fe and Mn oxides in the chambers were investigated by analyzing their XPS spectra. Figure 5 reveals Fe2p spectra of the iron oxides before and after reaction with As in the chambers. As shown in Figure 5c, Fe(III) was the dominant Fe species that existed on ferrihydrite surfaces, evidenced by the peak shape and the binding energy of ~ 711.0 eV [19, 42]. There was no obvious change of binding energy in Fe2p spectra when As(III) was added into ferrihydrite and Mn oxide chambers (Figure 5a and b). However, a decrease in Fe2p spectra intensity appeared after reaction with As (Figure 5a and b). This observation also appeared when As(III) was added into hematite and manganese oxide

chambers (Figure 5d and e), suggesting the existence of a strong interaction between Fe oxide and As species [19, 29, 43].

Mn2p spectra of Mn oxides before and after reaction with As(III) in the chambers is shown in Figure S9. With addition of As(III) into the Mn oxide chamber, the binding energy of Mn2p3/2 spectra decreased from 642.5 to 642.1 eV relative to fresh Mn oxide (Figure S9b and c). This may be explained by an increase in the fraction of reduced Mn species relative to Mn(IV) originating from As(III) oxidation by Mn oxide [44-46]. Addition of As(III) into the ferrihydrite chamber also decreased the binding energy of Mn2p3/2 spectra, indicating that there was partial diffusion of As(III) species into the Mn oxide chamber which subsequently reacted with Mn oxide to reduce the oxidation state of Mn species (Figure S9a). A decrease in binding energy, but with no obvious intensity change of Mn2p spectra in Mn oxide, was observed when addition of As(III) was added into both hematite and Mn oxide chambers (Figure S9d and e), suggesting that Mn oxide mainly responds to oxidation of As(III), rather than adsorption in this case.

Spectra for As3d species adsorbed by Fe and Mn oxides is shown in Figure 6. With addition of As(III) in the ferrihydrite chamber, As3d binding energy was ~ 44.3 eV (Figure 6a) [45, 46]. With As(III), the As3d binding energy significantly increased from ~ 44.3 to ~ 45.5 eV (Figure 6b). According to previous literature, As3d binding energy at 45.2 ~ 45.6 eV in arsenic oxide is attributed to As(V) species [19, 43, 44, 46]. This indicated that As(III) was rapidly oxidized to As(V) by Mn oxide, subsequently diffusing into the ferrihydrite chamber, followed by adsorption onto ferrihydrite. The main As species adsorbed by Mn oxide was As(V), evidenced by the As3d binding energy of ~ 45.5 eV (Figure 6a and b) [45]. However, the As3d spectra intensity of As species adsorbed by Mn oxide was lower than that of ferrihydrite, suggesting that Mn oxide was not responsible for As adsorption, which was consistent with

310 both adsorption isotherm data and Mn2p XPS spectra analysis. In the hematite chamber, As3d binding
311 energy was ~ 45.5 eV (Figure 6c). Arsenic species adsorbed by hematite were mainly As(V) (Figure 6a).
312 Unlike ferrihydrite, hematite adsorbed only a small amount of As(III). Unadsorbed As(III) slowly
313 diffused into the Mn oxide chamber and may subsequently have been oxidized to As(V). Total As
314 adsorbed by hematite was the same after the reaction reached equilibrium no matter which chamber
315 As(III) was added to, and was confirmed by As3d spectra intensity. This phenomenon also explained
316 why residual As concentrations were the same in the two Donnan experiments (Figure 4b). From the
317 above discussion, it may be concluded that As(III) oxidation mediated by manganese oxide in Fe-Mn
318 oxides is not suitable for all Fe-Mn binary oxides.
319 **Environmental Implications.** Fe-Mn binary oxides have been widely used as highly efficient absorbents
320 for application of As removal due to low-cost and environmental affability [47, 48]. Previous works have
321 suggested that synergistic effects between iron oxide as an absorbent and manganese oxide as an oxidant
322 are responsible for increasing As(III) removal [14, 19-22, 29]. However, in this study, we have revealed
323 both synergistic and antagonistic effects, in Fe-Mn binary oxides during As(III) removal. Arsenic-
324 synthesized Fe-Mn binary oxides under laboratory conditions usually have specific surface areas greater
325 than those of their corresponding single Fe and Mn oxides, and may exhibit more active sites for As
326 adsorption, consequently unintentionally masking the antagonistic effect of As(III) removal [24, 29]; this
327 phenomenon was confirmed in this study. Amorphous ferrihydrite is abundantly present in the natural
328 environment and has a high reactivity [23], which makes it an important adsorbent for As immobilization
329 in naturally reducing groundwater, sediment, and soil systems. As such the effect of Mn oxide on arsenite
330 adsorption on ferrihydrite should not be ignored, because both Fe and Mn oxides usually coexist in a
331 reducing environment. This potentially explains why As species are not completely adsorbed by iron

(hydr-)oxide in reduced groundwater. In addition, this finding provides a new insight into the working relationships between Fe and Mn oxides for As removal, which should aid in the rational design and adequate selection of highly efficient absorbents of Fe-Mn binary oxides for treating real As contaminated groundwater.

ASSOCIATED CONTENT

Supporting Information.

XRD, EDS data, SEM images, Langmuir and Freundlich isotherm parameters for As(III) and As(V), specific surface areas, FTIR spectra, aqueous arsenic concentration in Donnan reactor, Mn2p XPS spectra profiles of the samples are available free of charge via the Internet at http://pubs.acs.org.

AUTHOR INFORMATION

Corresponding Author

*Jingtao Hou; Email: houjt87@163.com

*Shuxin Tu; Email: stu@mail.hzau.edu.cn

Notes

The authors declare no competing financial interest.

ACKNOWLEDGMENT

This work was supported by National Natural Science Foundation of China (41571229, 41977022), National Key Research and Development Program of China (2018YFC1800305), Hubei Provincial Natural Science Foundation of China (2018CFB627), and the Fundamental Research Funds for the Central Universities (No. 2662017QD013).

REFERENCES

1. Smedley, P. L.; Kinniburgh, D. G., A review of the source, behaviour and distribution of arsenic in natural waters. Appl. Geochem. 2002, 17, (5), 517-568.
2. Choong, T. S.; Chuah, T.; Robiah, Y.; Koay, F. G.; Azni, I., Arsenic toxicity, health hazards and removal techniques from water: an overview. Desalination 2007, 217, (1-3), 139-166.
3. Edition, F., Guidelines for drinking-water quality. WHO chronicle 2011, 38, (4), 104-8.
4. Gorny, J.; Billon, G.; Lesven, L.; Dumoulin, D.; Made, B.; Noiriel, C., Arsenic behavior in river sediments under redox gradient: A review. Sci. Total Environ. 2015, 505, 423-434.
5. Gupta, K.; Bhattacharya, S.; Chattopadhyay, D.; Mukhopadhyay, A.; Biswas, H.; Dutta, J.; Ray, N. R.; Ghosh, U. C., Ceria associated manganese oxide nanoparticles: Synthesis, characterization and arsenic(V) sorption behavior. Chem. Eng. J. 2011, 172, (1), 219-229.
6. Gupta, K.; Bhattacharya, S.; Nandi, D.; Dhar, A.; Maity, A.; Mukhopadhyay, A.; Chattopadhyay, D. J.; Ray, N. R.; Sen, P.; Ghosh, U. C., Arsenic(III) sorption on nanostructured cerium incorporated manganese oxide (NCMO): A physical insight into the mechanistic pathway. J. Colloid Interface Sci. 2012, 377, 269-276.
7. Chen, J.; Wang, J. Y.; Zhang, G. S.; Wu, Q. Y.; Wang, D. T., Facile fabrication of nanostructured cerium-manganese binary oxide for enhanced arsenite removal from water. Chem. Eng. J. 2018, 334, 1518-1526.
8. Zhang, G. S.; Khorshed, A.; Chen, J. P., Simultaneous removal of arsenate and arsenite by a nanostructured zirconium-manganese binary hydrous oxide: Behavior and mechanism. J. Colloid Interface Sci. 2013, 397, 137-143.
9. Yin, Y. W.; Zhou, T. T.; Luo, H. J.; Geng, J. J.; Yu, W. Y.; Jiang, Z. J., Adsorption of arsenic by

activated charcoal coated zirconium-manganese nanocomposite: Performance and mechanism. Colloid Surf. A-Physicochem. Eng. Asp. 2019, 575, 318-328.

10. Cai, X. J.; Li, Y.; Guo, J. W.; Liu, S.; Na, P., Mn(IV) promotion mechanism for the photocatalytic oxidation of arsenite by anatase-TiO2. Chem. Eng. J. 2014, 248, 9-17.

11. Zhang, W.; Zhang, G. S.; Liu, C. H.; Li, J.; Zheng, T.; Ma, J.; Wang, L.; Jiang, J.; Zhai, X. D., Enhanced removal of arsenite and arsenate by a multifunctional Fe-Ti-Mn composite oxide: Photooxidation, oxidation and adsorption. Water Res. 2018, 147, 264-275.

12. Zhang, W.; Liu, C. H.; Zheng, T.; Ma, J.; Zhang, G. S.; Ren, G. H.; Wang, L.; Liu, Y. L., Efficient oxidation and sorption of arsenite using a novel titanium(IV)-manganese(IV) binary oxide sorbent. J. Hazard. Mater. 2018, 353, 410-420.

13. Li, X.; He, K.; Pan, B. C.; Zhang, S. J.; Lu, L.; Zhang, W. M., Efficient As(III) removal by macroporous anion exchanger-supported Fe-Mn binary oxide: Behavior and mechanism. Chem. Eng. J. 2012, 193, 131-138.

14. Zhang, G. S.; Liu, H. J.; Qu, J. H.; Jefferson, W., Arsenate uptake and arsenite simultaneous sorption and oxidation by Fe-Mn binary oxides: Influence of Mn/Fe ratio, pH, Ca2+, and humic acid. J. Colloid Interface Sci. 2012, 366, (1), 141-146.

15. Zhu, J.; Baig, S. A.; Sheng, T. T.; Lou, Z. M.; Wang, Z. X.; Xu, X. H., Fe3O4 and MnO2 assembled on honeycomb briquette cinders (HBC) for arsenic removal from aqueous solutions. J. Hazard. Mater. 2015, 286, 220-228.

16. Xu, F. N.; Chen, H. X.; Dai, Y. X.; Wu, S. L.; Tang, X. J., Arsenic adsorption and removal by a new starch stabilized ferromanganese binary oxide in water. J. Environ. Manage. 2019, 245, 160-167.

17. Wu, K.; Liu, T.; Xue, W.; Wang, X. C., Arsenic(III) oxidation/adsorption behaviors on a new bimetal adsorbent of Mn-oxide-doped Al oxide. Chem. Eng. J. 2012, 192, 343-349.

18. Wu, K.; Zhang, N.; Liu, T.; Ma, C.; Jin, P. K.; Zhang, F. R.; Zhang, J.; Wang, X. C., Competitive adsorption behaviors of arsenite and fluoride onto manganese-aluminum binary adsorbents. Colloid Surf. A-Physicochem. Eng. Asp. 2017, 529, 185-194.

19. Zhang, G. S.; Qu, J. H.; Liu, H. J.; Liu, R. P.; Li, G. T., Removal mechanism of As(III) by a novel Fe-Mn binary oxide adsorbent: Oxidation and sorption. Environ. Sci. Technol. 2007, 41, (13), 4613-4619.

20. Zhang, G. S.; Liu, H. J.; Liu, R. P.; Qu, J. H., Adsorption behavior and mechanism of arsenate at Fe-Mn binary oxide/water interface. J. Hazard. Mater. 2009, 168, (2-3), 820-825.

21. Ocinski, D.; Jacukowicz-Sobala, I.; Mazur, P.; Raczyk, J.; Kociolek-Balawejder, E., Water treatment residuals containing iron and manganese oxides for arsenic removal from water - Characterization of physicochemical properties and adsorption studies. Chem. Eng. J. 2016, 294, 210-221.

22. Bai, Y. H.; Yang, T. T.; Liang, J. S.; Qu, J. H., The role of biogenic Fe-Mn oxides formed in situ for arsenic oxidation and adsorption in aquatic ecosystems. Water Res. 2016, 98, 119-127.

23. Raven, K. P.; Jain, A.; Loeppert, R. H., Arsenite and arsenate adsorption on ferrihydrite: Kinetics, equilibrium, and adsorption envelopes. Environ. Sci. Technol. 1998, 32, (3), 344-349.

24. Zhang, G. S.; Liu, F. D.; Liu, H. J.; Qu, J. H.; Liu, R. P., Respective Role of Fe and Mn Oxide Contents for Arsenic Sorption in Iron and Manganese Binary Oxide: An X-ray Absorption Spectroscopy Investigation. Environ. Sci. Technol. 2014, 48, (17), 10316-10322.

25. Wen, Z. P.; Zhang, Y. L.; Zhou, X. F.; Chen, R., Effective As(III) and As(V) immobilization

from aqueous solution by nascent ferrous hydroxide colloids (FHC). Sep. Purif. Technol. 2017, 176, 395-401.

26. Kong, S. Q.; Wang, Y. X.; Hu, Q. H.; Olusegun, A. K., Magnetic nanoscale Fe-Mn binary oxides loaded zeolite for arsenic removal from synthetic groundwater. Colloid Surf. A-Physicochem. Eng. Asp. 2014, 457, 220-227.

27. Cui, H. J.; Cai, J. K.; Zhao, H.; Yuan, B. L.; Ai, C. L.; Fu, M. L., Fabrication of magnetic porous Fe-Mn binary oxide nanowires with superior capability for removal of As(III) from water. J. Hazard. Mater. 2014, 279, 26-31.

28. McCann, C. M.; Peacock, C. L.; Hudson-EdWards, K. A.; Shrimpton, T.; Gray, N. D.; Johnson, K. L., In situ arsenic oxidation and sorption by a Fe-Mn binary oxide waste in soil. J. Hazard. Mater. 2018, 342, 724-731.

29. Zhang, G. S.; Qu, J. H.; Liu, H. J.; Liu, R. P.; Wu, R. C., Preparation and evaluation of a novel Fe-Mn binary oxide adsorbent for effective arsenite removal. Water Res. 2007, 41, (9), 1921-1928.

30. Ying, S. C.; Kocar, B. D.; Fendorf, S., Oxidation and competitive retention of arsenic between iron- and manganese oxides. Geochim. Cosmochim. Acta 2012, 96, 294-303.

31. Redman, A. D.; Macalady, D. L.; Ahmann, D., Natural organic matter affects arsenic speciation and sorption onto hematite. Environ. Sci. Technol. 2002, 36, (13), 2889-2896.

32. Hong, J.; Liu, L. H.; Luo, Y.; Tan, W. F.; Qiu, G. H.; Liu, F., Photochemical oxidation and dissolution of arsenopyrite in acidic solutions. Geochim. Cosmochim. Acta 2018, 239, 173-185.

33. Tang, W. S.; Li, Q.; Gao, S. A.; Shang, J. K., Arsenic (III,V) removal from aqueous solution by ultrafine alpha-Fe2O3 nanoparticles synthesized from solvent thermal method. J. Hazard. Mater. 2011, 192, (1), 131-138.

34. Manning, B. A.; Fendorf, S. E.; Bostick, B.; Suarez, D. L., Arsenic(III) oxidation and arsenic(V) adsorption reactions on synthetic birnessite. Environ. Sci. Technol. 2002, 36, (5), 976-981.

35. Lafferty, B. J.; Ginder-Vogel, M.; Zhu, M. Q.; Livi, K. J. T.; Sparks, D. L., Arsenite Oxidation by a Poorly Crystalline Manganese-Oxide. 2. Results from X-ray Absorption Spectroscopy and X-ray Diffraction. Environ. Sci. Technol. 2010, 44, (22), 8467-8472.

36. Hou, J. T.; Luo, J. L.; Hu, Z. Q.; Li, Y. Z.; Mao, M. Y.; Song, S. X.; Liao, Q. L.; Li, Q. Z., Tremendous effect of oxygen vacancy defects on the oxidation of arsenite to arsenate on cryptomelane-type manganese oxide. Chem. Eng. J. 2016, 306, 597-606.

37. Hou, J. T.; Xiang, Y. J.; Zheng, D.; Li, Y. Z.; Xue, S. G.; Wu, C.; Hartley, W.; Tan, W. F., Morphology-dependent enhancement of arsenite oxidation to arsenate on birnessite-type manganese oxide. Chem. Eng. J. 2017, 327, 235-243.

38. Voegelin, A.; Hug, S. J., Catalyzed oxidation of arsenic(III) by hydrogen peroxide on the surface of ferrihydrite: An in situ ATR-FTIR study. Environ. Sci. Technol. 2003, 37, (5), 972-978.

39. Parikh, S. J.; Lafferty, B. J.; Sparks, D. L., An ATR-FTIR spectroscopic approach for measuring rapid kinetics at the mineral/water interface. J. Colloid Interface Sci. 2008, 320, (1), 177-185.

40. Lan, S.; Ying, H.; Wang, X. M.; Liu, F.; Tan, W. F.; Huang, Q. Y.; Zhang, J.; Feng, X. H., Efficient catalytic As(III) oxidation on the surface of ferrihydrite in the presence of aqueous Mn(II). Water Res. 2018, 128, 92-101.

41. Hou, J. T.; Sha, Z. J.; Hartley, W.; Tan, W. F.; Wang, M. X.; Xiong, J.; Li, Y. Z.; Ke, Y. J.; Long, Y.; Xue, S. G., Enhanced oxidation of arsenite to arsenate using tunable K+ concentration in the OMS-2 tunnel. Environ. Pollut. 2018, 238, 524-531.

42. Wen, Z. P.; Zhang, Y. L.; Wang, Y.; Li, L. N.; Chen, R., Redox transformation of arsenic by

magnetic thin-film MnO2 nanosheet-coated flowerlike Fe3O4 nanocomposites. Chem. Eng. J. 2017, 312, 39-49.

43. Zhang, Y.; Yang, M.; Dou, X. M.; He, H.; Wang, D. S., Arsenate adsorption on an Fe-Ce bimetal oxide adsorbent: Role of surface properties. Environ. Sci. Technol. 2005, 39, (18), 7246-7253.

44. Nesbitt, H. W.; Canning, G. W.; Bancroft, G. M., XPS study of reductive dissolution of 7 angstrom-birnessite by H3AsO3, with constraints on reaction mechanism. Geochim. Cosmochim. Acta 1998, 62, (12), 2097-2110.

45. Lafferty, B. J.; Ginder-Vogel, M.; Sparks, D. L., Arsenite Oxidation by a Poorly-Crystalline Manganese Oxide. 3. Arsenic and Manganese Desorption. Environ. Sci. Technol. 2011, 45, (21), 9218-9223.

46. Hou, J. T.; Luo, J. L.; Song, S. X.; Li, Y. Z.; Li, Q. Z., The remarkable effect of the coexisting arsenite and arsenate species ratios on arsenic removal by manganese oxide. Chem. Eng. J. 2017, 315, 159-166.

47. Chakravarty, S.; Dureja, V.; Bhattacharyya, G.; Maity, S.; Bhattacharjee, S., Removal of arsenic from groundwater using low cost ferruginous manganese ore. Water Res. 2002, 36, (3), 625-632.

48. Chang, F. F.; Qu, J. H.; Liu, R. P.; Zhao, X.; Lei, P. J., Practical performance and its efficiency of arsenic removal from groundwater using Fe-Mn binary oxide. J. Environ. Sci. 2010, 22, (1), 1-6.

Table and Figure Captions:

Figure 1. Schematic illustration of the Donnan reactor composed of two reaction cells separated by a semi-permeable membrane, where Fe and Mn oxides were placed into two chambers, respectively.

Figure 2. Adsorption isotherms for As(III) and As(V) by hematite (a), goethite (b), ferrihydrite (c), the

484 mixtures of hematite and MnO_x (d), goethite and MnO_x (e), and ferrihydrite and MnO_x (f) with a 100

485 mg L^{-1} suspension at pH 7.0.

486 **Figure 3.** Time-dependence of in suit flow ATR-FTIR spectra of ferrihydrite (a), hematite (b), the

487 mixed ferrihydrite and MnO_x (c), and the mixed hematite and MnO_x (d) reacted with 1 mM of As(III)

488 solution at pH 7.0.

489 **Figure 4.** The evolution of aqueous arsenic concentration in Fe and Mn oxide chambers as a function

490 of time within ferrihydrite-Mn oxide (a, b) and hematite-Mn oxide (c, d) systems at pH= 7. The dosage

491 of Fe and Mn oxides in chambers was 100 mg L^{-1}. The As(III) concentration added in ferrihydrite-Mn

492 oxide and hematite-Mn oxide systems was 133.3 and 26.7 μM, respectively.

493 **Figure 5.** The Fe2p XPS spectra of the iron oxides in ferrihydrite-Mn oxide (a, b, c) and hematite-Mn

494 oxide (d, e, f) systems before and after adding As(III) in Fe or Mn oxides chambers.

495 **Figure 6.** The As3d XPS spectra of the arsenic species adsorbed by iron or Mn oxides in ferrihydrite-

496 Mn oxide (a, b) and hematite-Mn oxide (c, d) systems after adding As(III) into Fe or Mn oxide

497 chambers.

498

499

500

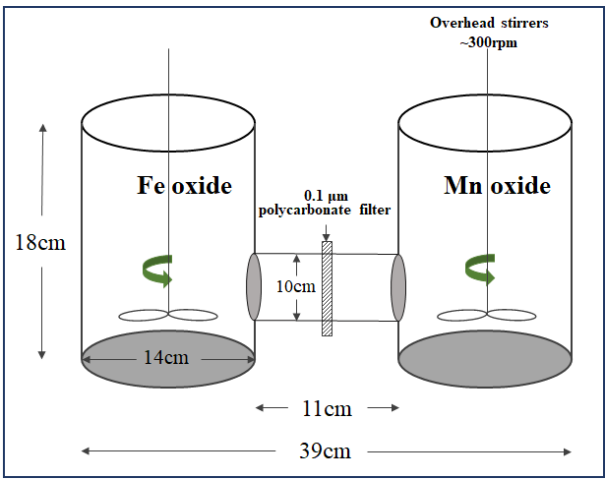

Figure 1. Schematic illustration of the Donnan reactor composed of two reaction cells separated by a semi-permeable membrane, where Fe and Mn oxides were placed into two chambers, respectively.

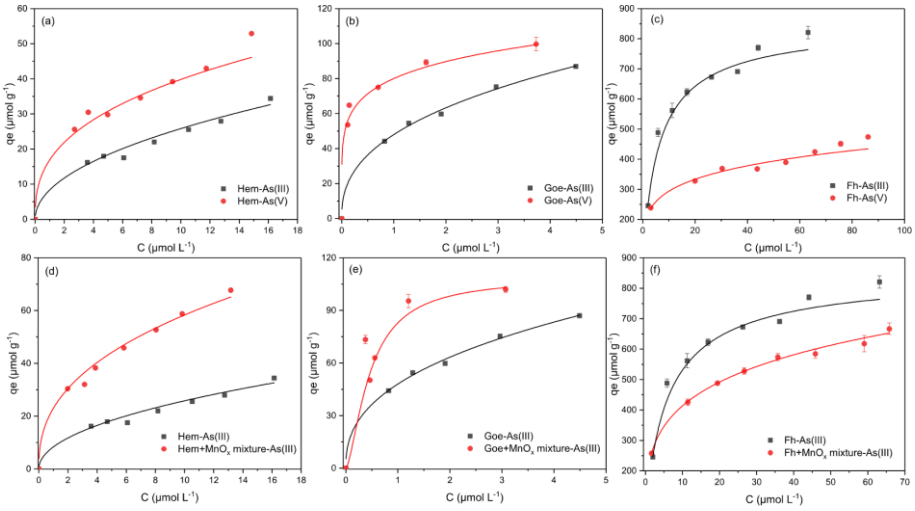

Figure 2. Adsorption isotherms for As(III) and As(V) by hematite (a), goethite (b), ferrihydrite (c), mixtures of hematite and MnO_x (d), goethite and MnO_x (e), and ferrihydrite and MnO_x (f) with a 100 mg L^{-1} suspension at pH 7.0.

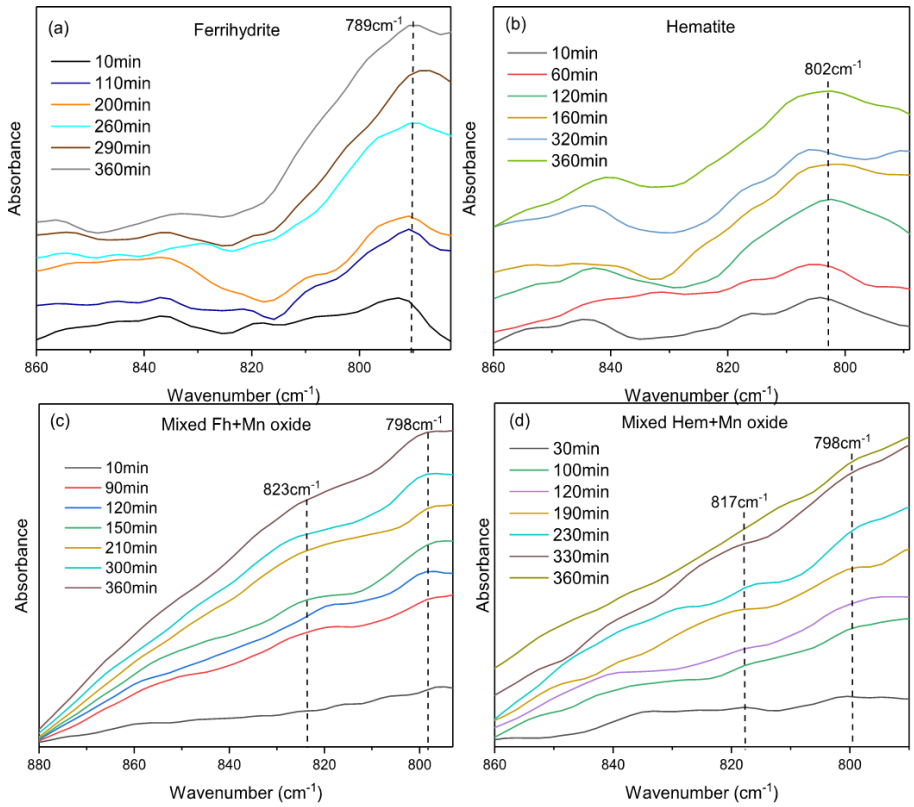

Figure 3. Time-dependence of in suit flow ATR-FTIR spectra of ferrihydrite (a), hematite (b), mixed ferrihydrite and MnO_x (c), mixed hematite and MnO_x (d) reacted with 1 mM of As(III) solution at pH 7.0.

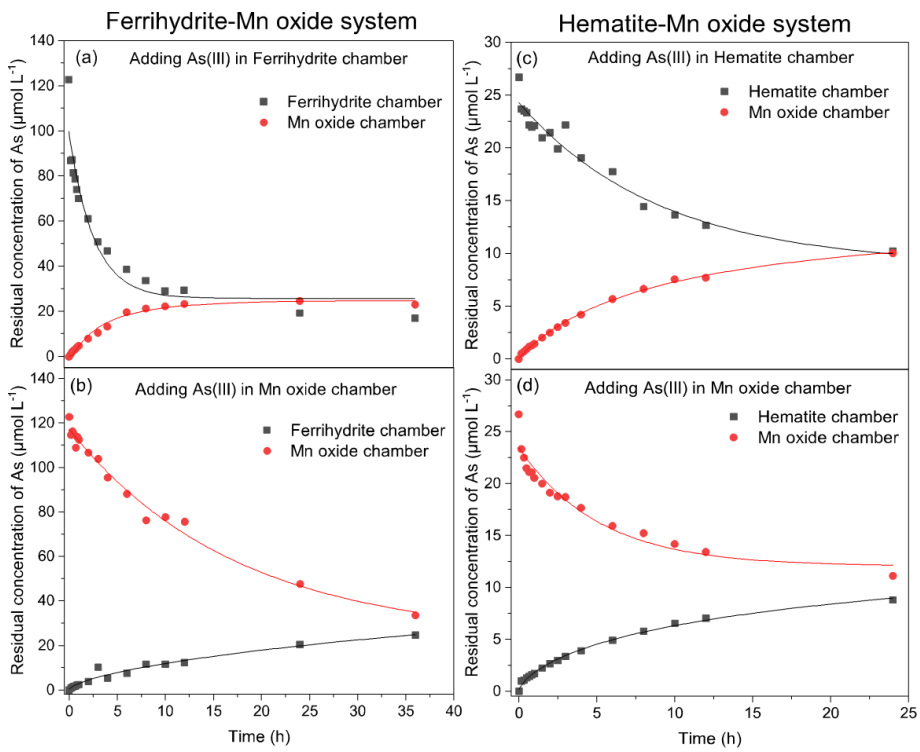

Figure 4. Evolution of aqueous As concentration in Fe and Mn oxide chambers as a function of time within ferrihydrite-Mn oxide (a, b) and hematite-Mn oxide (c, d) systems at pH= 7. The dosage of Fe and Mn oxides in chambers was 100 mg L^{-1}. The As(III) concentration added in ferrihydrite-Mn oxide and hematite-Mn oxide systems was 133.3 and 26.7 μM, respectively.

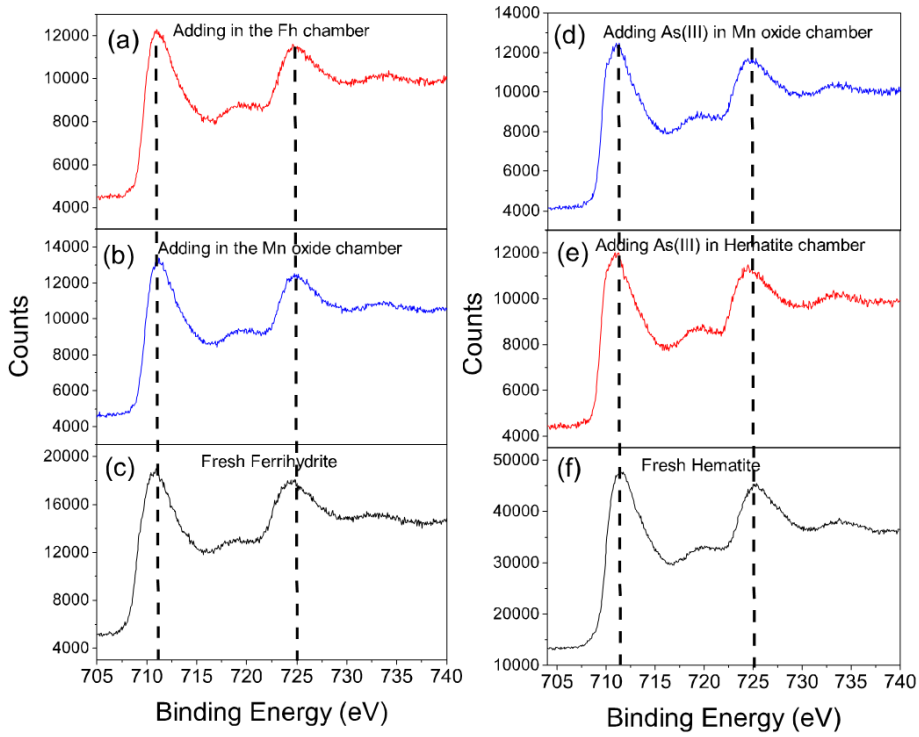

Figure 5. Fe2p XPS spectra of iron oxides in ferrihydrite-Mn oxide (a, b, c) and hematite-Mn oxide (d, e, f) systems before and after adding As(III) in Fe or Mn oxide chambers.

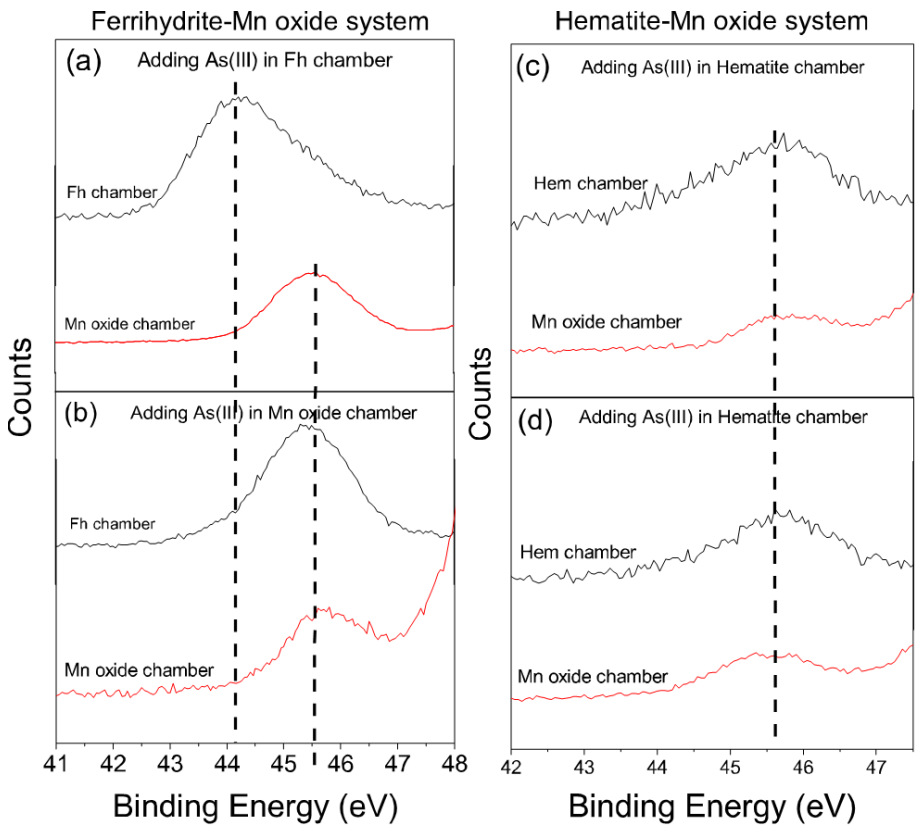

Figure 6. As3d XPS spectra of As species adsorbed by iron or Mn oxides in ferrihydrite-Mn oxide (a, b) and hematite-Mn oxide (c, d) systems after adding As(III) into Fe or Mn oxide chambers.

Supporting Information

As(III) adsorption on Fe-Mn binary oxides: Are manganese oxide and iron oxide synergistic or antagonistic for arsenic removal?

Qian Zheng,[†] Jingtao Hou,[†,*] Mingxia Wang,[†] Shuxin Tu,[†,*] Wenfeng Tan[†]

College of Resources and Environment, Huazhong Agricultural University, Wuhan 430070, China.

Pages: 4

Tables: 3

Figures: 6

***Corresponding author**: *Jingtao Hou; Email: houjt87@163.com

*Shuxin Tu; Email: stu@mail.hzau.edu.cn

Table S1. EDS data of Fe and Mn elemental content in different Fe-Mn binary oxides.

Fe-Mn binary oxides	Elements							
	Fe K		Mn K		C k		O K	
	Weight (%)	Atomic (%)	Weight (%)	Atomic (%)	Weight (%)	Atomic (%)	Weight (%)	Atomic (%)
Hem-MnO_x	38.09	17.12	14.75	6.74	4.09	8.54	43.07	67.59
Goe-MnO_x	69.66	56.29	20.59	16.91	0.58	0.93	9.17	25.87
Fh-MnO_x	44.87	21.01	11.34	5.4	3.67	8	40.12	65.59

Table S2. Specific surface areas (SSA) of the samples.

Samples	Specific surface areas (m^2 g^{-1})
Hematite	38.9
Goethite	143.3
Ferrihydrite	247.0*
Manganese oxide	46.5
Hem-MnO_x	32.8
Goe-MnO_x	213.3
Fh-MnO_x	266.4

*Data was cited from previous work reported by Zhang et al (J Hazard. Mater. 2009, 168, 820-825).

Table S3. Langmuir and Freundlich isotherm parameters for As(III) and As(V) adsorption on single iron oxide, manganese oxide, Fe–Mn binary oxides, and mixed Fe and Mn oxides at pH 7.0.

As species	Adsorbents	Langmuir model			Freundlich model		
		q_m (μmol g^{-1})	b (L mol^{-1})	R^2	K_F (L mol^{-1})	n	R^2
As(III)	Hematite	51.2	1.4	0.892	2.2	0.5	0.942
	Goethite	112.8	0.1	0.988	10.1	0.4	0.991
	Ferrihydrite	871.5	2.1	0.993	40.3	0.3	0.917
	MnO_x	9.5	4.1	0.533	2.5	0.9	0.913
	Mixed Hem+MnO_2	90.7	2.6	0.969	4.5	0.5	0.977
	Mixed Goe+MnO_2	116.3	33.7	0.981	11.9	0.3	0.644
	Mixed Fh+MnO_2	694.4	2.0	0.989	33.0	0.3	0.996
	Binary Hem-MnO_x oxide	102.3	4.3	0.989	6.8	0.4	0.996
	Binary Goe-MnO_x oxide	131.5	33.8	0.997	10.1	0.2	0.988
	Binary Fh-MnO_x oxide	883.1	2.3	0.980	44.1	0.3	0.983
As(V)	Hematite	65.3	2.6	0.930	3.5	0.4	0.934
	Goethite	102.7	81.2	0.997	9.2	0.2	0.946
	Ferrihydrite	493.9	1.4	0.976	23.3	0.2	0.963
	MnO_x	2.8	0.01	0.844	7.9	0.6	0.938

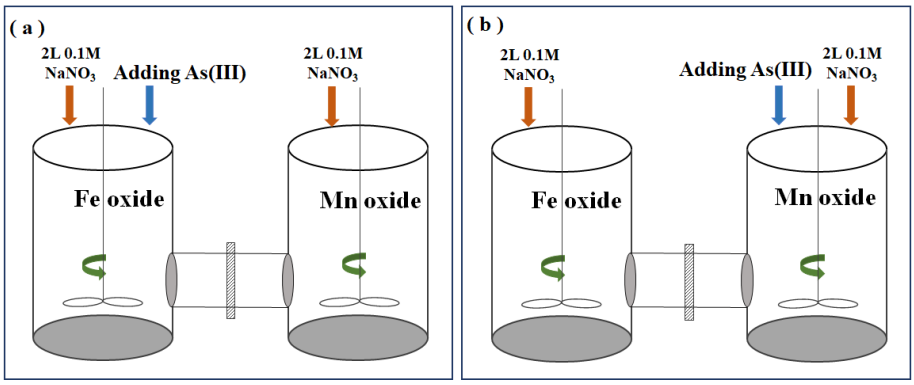

Figure S1. Schematic illustration of addition of As(III) solution into Fe oxide (a) and Mn oxide (b) chambers, respectively.

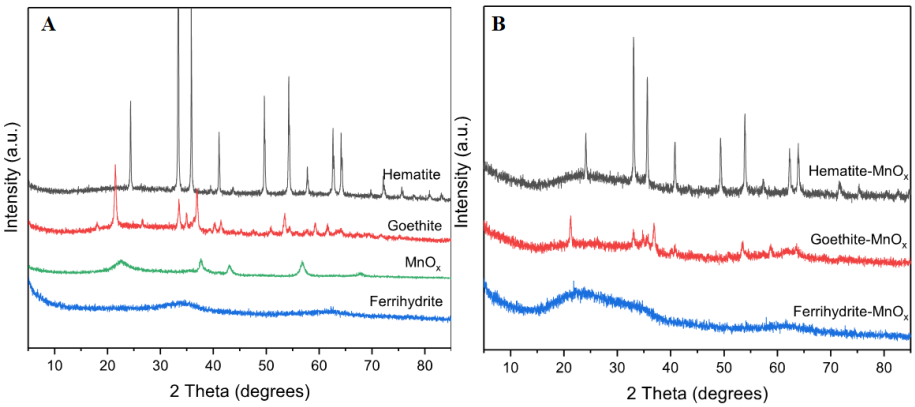

Figure S2. The XRD patterns of iron oxides and manganese oxide (A) and the corresponding Fe-Mn binary oxides (B).

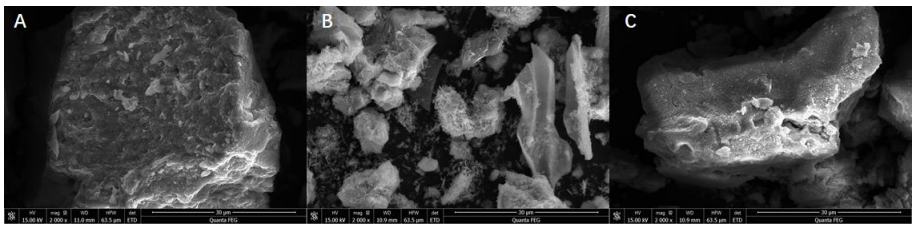

Figure S3. SEM morphology of ferrihydrite- (A), goethite-(B), and hematite-(C) containing Fe-Mn binary oxides.

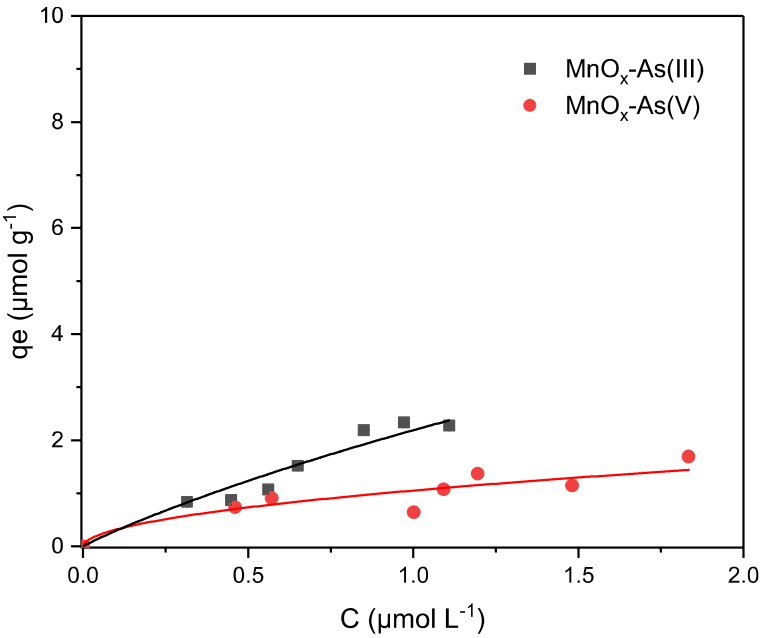

Figure S4. Adsorption isotherms for As(III) and As(V) by manganese oxide with a 100 mg L^{-1} suspension at pH 7.0.

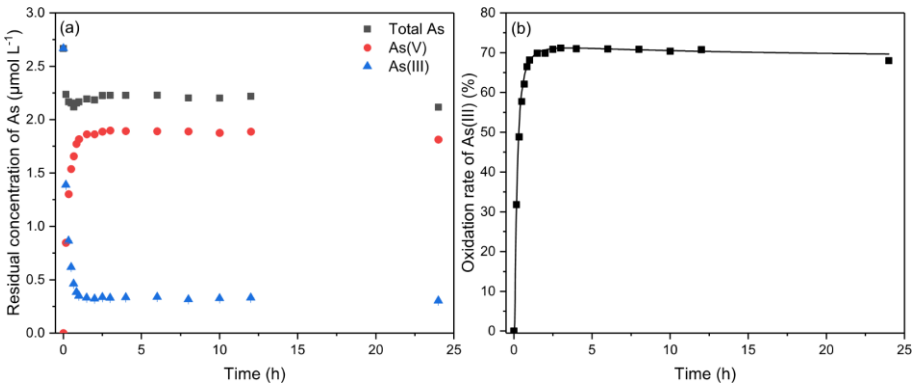

Figure S5. Evolution of the aqueous concentration of arsenic species (a) and the As(III) oxidation rate (b) with reaction time at pH 7.0. Initial As(III) concentration was 2.67 μmol L^{-1}; Manganese oxide dosage was 100 mg L^{-1}.

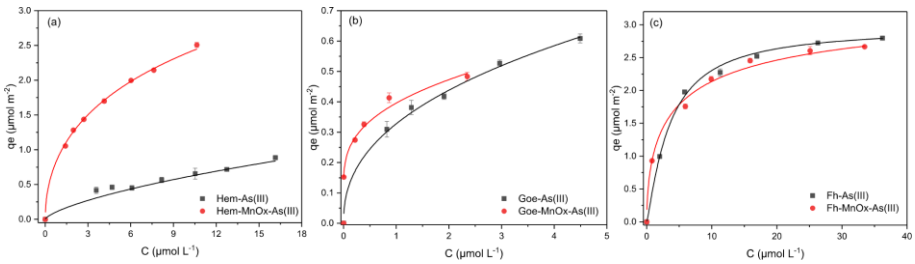

Figure S6. Adsorption isotherms for As(III) by different Fe-Mn binary oxides with a 0.2 mg L^{-1} dosage at pH 7.0. All the data were normalized by specific surface areas.

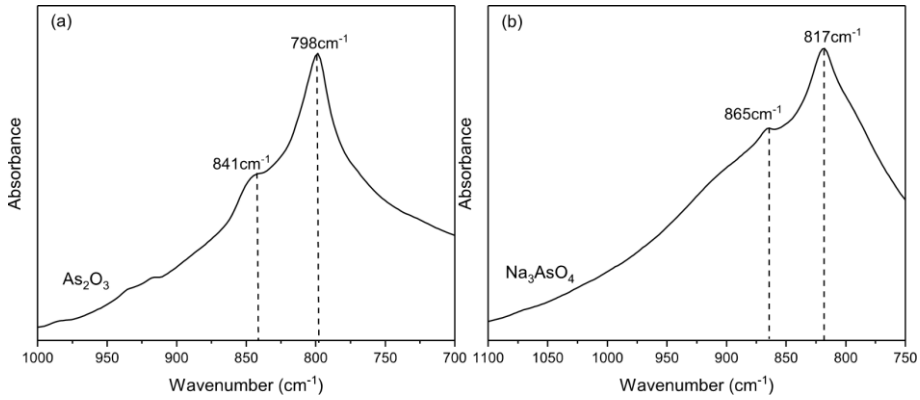

Figure S7. FTIR spectra of As(III) (a) and As(V) (b) standards.

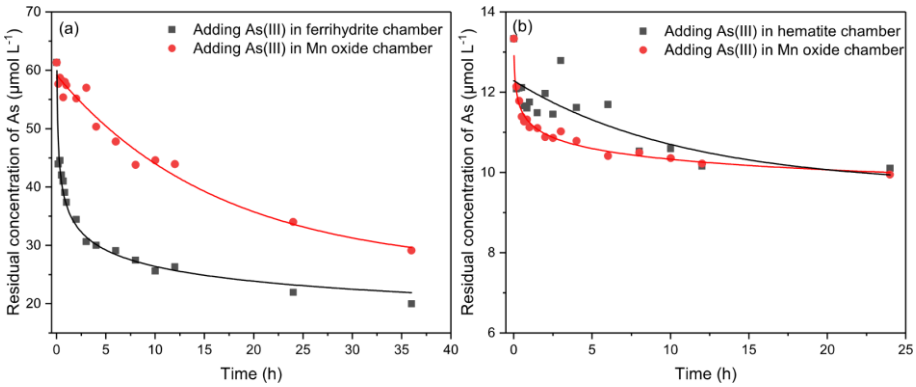

Figure S8. Evolution of aqueous arsenic concentration as a function of time in ferrihydrite-Mn oxide (a) and hematite-Mn oxide (b) systems after adding As(III) into Fe or Mn oxides chambers.

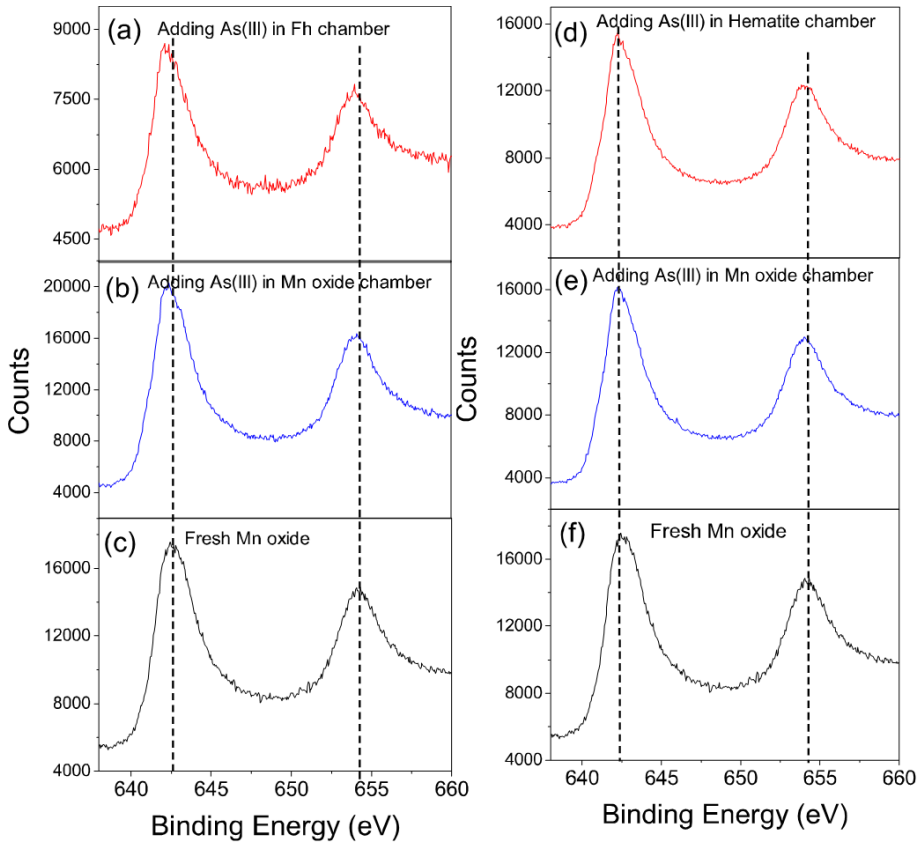

Figure S9. Mn2p XPS spectra of the Mn oxides in ferrihydrite-Mn oxide (a, b, c) and hematite-Mn oxide (d, e, f) systems before and after adding As(III) in Fe or Mn oxide chambers.